Appels, W. M., Graham, C. B., Freer, J. E., & Mcdonnell, J. J. (2015). Factors affecting the spatial pattern of bedrock groundwater recharge at the hillslope scale. Journal of Hydrology, 29(21), 4594-4610. DOI: 10.1002/hyp.10481

Factors affecting the spatial pattern of bedrock groundwater recharge at the hillslope scale

Running head: Spatial patterns of bedrock groundwater recharge

Keywords: groundwater recharge, spatial patterns, conceptual modeling

Corresponding author: Willemijn M. Appels, Global Institute for Water Security, University of Saskatchewan, Saskatoon CANADA (willemijn.appels@usask.ca)

Chris B. Graham, Hetchy Hetchy Water and Power, Moccassin, CA USA (chris.b.graham@gmail.com)

Jim E. Freer, School of Geographical Sciences, University of Bristol, Bristol UK (jim.freer@bristol.ac.uk)

Jeffrey J. McDonnell, Global Institute for Water Security, University of Saskatchewan, Saskatoon CANADA; School of Geosciences, University of Aberdeen, Aberdeen, Scotland UK; Dept of Forest Engineering, Resources and Management, Oregon State University, Corvallis OR USA (jeffrey.mcdonnell@usask.ca)

Abstract

The spatial patterns of groundwater recharge on hillslopes with a thin soil mantle overlying bedrock are poorly known. Complex interactions between vertical percolation of water through the soil, permeability contrasts between soil and bedrock, and lateral redistribution of water result in large spatial variability of water moving into the bedrock. Here, we combine new measurements of saturated hydraulic conductivity of soil mantle and bedrock of the well-studied Panola Mountain experimental hillslope with previously collected (sub)surface topography and soil depth data to quantify the factors affecting the spatial pattern of bedrock groundwater recharge.

We use geostatistical characteristics of the measured permeability to generate spatial fields of saturated hydraulic conductivity for the entire hillslope. We perform simulations with a new conceptual model with these random fields and evaluate the resulting spatial distribution of groundwater recharge during individual rainstorms and series of rainfall events. Our simulations show that unsaturated drainage from soil into bedrock is the prevailing recharge mechanism and accounts for 60% of annual groundwater recharge. Therefore, soil depth is a major control on the groundwater recharge pattern through available storage capacity and controlling the size of vertical flux. The other 40% of recharge occurs during storms that feature transient saturation at the soil-bedrock interface. Under these conditions, locations that can sustain increased subsurface saturation due to their topographical characteristics or those with high bedrock permeability will act as hotspots of groundwater recharge when they receive lateral flow.

1. Introduction

The hierarchy of controls on patterns of groundwater recharge at varying spatial scales is poorly understood (Scanlon *et al*., 2002). At the regional and watershed scale, where groundwater recharge is the renewable resource of large aquifers, recent research has demonstrated the vulnerability of groundwater recharge due to land use and climate change (Barron *et al*., 2012; Flint *et al*., 2014; Mair *et al*., 2013). At smaller spatial scales of 1-10 m^2, lysimeter and tracer studies have shown large temporal variation in such point scale recharge fluxes under different climate regimes (Pangle *et al*., 2014; Allison *et al*., 1994).

Few investigations have yet examined hillslope-scale controls on the spatio-temporal variability of groundwater recharge. This is problematic because hillslopes are the fundamental hydrological unit (Troch *et al*., 2013) and the scale at which flow accumulation occurs in the landscape. Therefore a key challenge in groundwater recharge research is the prediction and assessment of its variability at the hillslope scale (Allison *et al*., 1994; De Vries and Simmers, 2002). Though spatial variability of groundwater recharge at hillslope scale may not be critical for water resource management (Flint *et al*., 2012), it may have profound implications for solute and contaminant transport. Zones of focused recharge can allow contaminants to move quickly from the unsaturated zone to underlying aquifers and streams (Scanlon *et al*., 2002). Here we define hillslope groundwater recharge as all water that is transferred from the soil into the bedrock, where it is no longer available for root water uptake. At the hillslope scale, such recharge may feed aquifers through deep percolation, but also fast flow through fractures that may contribute to catchment streamflow farther down-valley (Torres *et al*., 1997; Montgomery *et al*., 2002; Gleeson *et al*., 2009; Graham *et al*., 2010; Gabrielli *et al*., 2012).

Groundwater recharge can be a substantial part of the water balance partitioning between vertical and lateral flow. Heppner *et al*. (2007) measured a range of 21% to 52% of annual rainfall under a grass lysimeter during five years of natural rainfall conditions. Experiments on small hillslopes have estimated groundwater recharge of 34-41% (Ontario,Canada; Buttle and McDonald, 2002), 41% (Oregon, USA; Graham *et al*., 2010), 35-55% (Japan; Kosugi *et al.*, 2006) and 94% (Georgia, USA; Tromp-van Meerveld *et al*., 2007), while runoff ratios on these hillslopes have been estimated to be respectively 30-43% (Peters *et al*., 1995), 13% (Gabrielli *et al.*, 2012), 3.5-7.4% (Kosugi *et al.*, 2006) and 5% (Tromp-van Meerveld and McDonnell, 2006a).
In other words, depending on the nature and variability of the soil-bedrock interface, the volume of water that moves vertically past the soil-bedrock interface can be equal to or larger than the volume of water that is routed laterally downslope along that interface. These relative values depend mainly on bedrock permeability, soil depth and slope angle (Asano *et al*., 2002; Hopp and McDonnell, 2009; Ebel and Loague, 2008). While experimental studies have shown that return flow from bedrock into soil can be caused by variability of bedrock conductivity (Wilson and Dietrich, 1987; Shand *et al.*, 2007) and hillslopes rarely experience a uniformly rising and falling perched groundwater table at the soil-bedrock interface (Salve *et al.*, 2012), the effects of spatial variability of hydraulic conductivity on groundwater recharge have not been quantified. The filling, leakage and lateral spilling of the hillslope-scale patches of transient saturation at the soil-bedrock interface are now seen as a common behavior across many environments (Bachmair and Weiler, 2011; McDonnell, 2013). However, the groundwater recharge consequences of this behavior have not yet been examined.

We present new measurements and new model results from the well-described Panola experimental hillslope (see Tromp-van Meerveld and McDonnell (2009) for a site review) to examine the hierarchy of factors affecting the spatial pattern of bedrock groundwater recharge. Considering the known bedrock topography and bedrock permeability at this hillslope, we hypothesize that saturation at the soil-bedrock interface (SBI) is a driver of increased bedrock groundwater recharge (GWR). We further hypothesize that rainfall dynamics are an important on/off switch for groundwater recharge patterns. We developed a new model (building upon Appels *et al.* (2011)) to examine a number of specific questions:

- How do spatial patterns of soil- and bedrock hydraulic conductivity (derived from new point-scale measurements) influence hillslope-scale transient soil saturation and resulting bedrock groundwater recharge?
- What is the sequence of controls on the spatial pattern of groundwater recharge?
- How do within- and between-storm rainfall conditions influence this sequencing and ultimate process hierarchy?

2. Study Site

The study hillslope is part of the Panola Mountain Research Watershed (PMRW), located in the Georgia Piedmont, southeast of Atlanta (GA, USA). In 1995, a 29x51 m hillslope was instrumented with 135 crest-stage gauges, 29 recording wells, and a 20 m wide trench at the downhill boundary, excavated down to competent bedrock. Detailed site and instrumentation descriptions can be found elsewhere (Freer *et al*., 2002; Tromp-van Meerveld and McDonnell, 2006a; 2006b; 2007; 2009). Here, we only describe the soil and bedrock characteristics that are relevant for the current modeling study.

The PMRW is underlain by Panola Granite bedrock, a 300 to 360 Ma old biotite-oligioclase-quartz-microcline granite formation. The primary conductivity of the granite matrix is estimated to be $7x10^{-6}$ m yr^{-1}, with a secondary regolith conductivity of $1x10^{-3}$ m yr^{-1} (White *et al*., 2001). The effective hydraulic conductivity of the weathered granite was found to be in the range of $8.8x10^{-8}$ to $5.1x10^{-6}$ m s^{-1} in falling head experiments (White *et al*., 2002) and $1.6x10^{-6}$ m s^{-1} in an area-average sprinkling experiment (Tromp-van Meerveld *et al*., 2007).
Throughout the watershed, the top 2 to 4 m of the bedrock is weathered to porous soft disintegrated granite (saprolite) that has retained the original granodiorite texture (White *et al*., 2001). Tromp-van Meerveld *et al*. (2007) did not find saprolite at the monitored hillslope site, except at the deepest soil section, 20-22 m upslope from the trench face (Fig. 1).

The soil depth ranges from 0.0 to 1.8 m (average 0.63 m) and consists of hillslope sediments and colluvium from upslope erosion (Freer *et al*., 1997; White *et al*., 2001; Tromp-van Meerveld *et al*., 2007). The coarse sandy loam does not have pronounced layering or discernible structure except for a 0.15 m thick organic horizon (Tromp-van Meerveld and McDonnell, 2006a). A large part of subsurface flow captured at the hillslope trench at the slope base takes place in macropores and soil pipes (Freer *et al*., 2002; Tromp-van Meerveld and McDonnell, 2006b).

Average seasonal hillslope runoff coefficients for fall, winter, spring, and summer periods are 6, 10, 1, <1 % respectively, resulting in a yearly average hillslope runoff coefficient of 5 % (Tromp-van Meerveld and McDonnell, 2006a). Accounting for evapotranspiration by the oak-hickory forest, groundwater recharge losses to the bedrock are greater than 20% of precipitation during large storm events, reaching 90 to 95% during artificial sprinkling events (Tromp-van Meerveld *et al*., 2007). Overland flow does not occur on the hillslope, except on the small section of exposed bedrock.

3. Methods

3.1 Measurements of saturated hydraulic conductivity of soil and bedrock

We measured vertical soil hydraulic conductivity in two transects of 240 and 285 m length with a Guelph permeameter at a maximum of four depths (0.19, 0.32, 0.46, 0.75 m). The transects were located perpendicular to the main stream channel downhill of the study site in a ridge and hollow on the hillslope. Each transect featured four measurement sites.

Lateral saturated hydraulic conductivity of the soil immediately above the bedrock was measured through falling head well tests in 135 wells, forming a very approximate 2x2 m grid (Fig. 1b). The wells were composed of 1.9 cm PVC pipes, augered to bedrock and screened over the bottom 0.10 m. A 1L bottle was fixed to the top of the well and the time needed to drain the 1L bottle was recorded. This experiment was repeated until steady state conditions were reached. Some wells were positioned in areas with either soil pipes or cracks and water could not be supplied at a rate high enough to quantify drawdown. No lateral saturated conductivity could be calculated from these wells.
The lateral conductivity was calculated by considering the drawdown from the bottles as a slug test:

$$Q = \frac{2\pi L_I K_L}{\ln(R_E/R_{W})} \quad (1)$$

The rate of water level change is related to the flux as:

$$\frac{dy}{dt} = \frac{-Q}{\pi R_C^2} \quad (2)$$

Combining equation 1 and 2 and integrating between the limits y_0 at time=0 and y_t at time = t, yields:

$$K_L = R_C^2 \ln(y_0/y_t)/Ft \quad (3)$$

Where F is a shape factor depending on the well geometry. The calculated K_L combines both effects of conductivity and the local bedrock gradient. We analyzed the results to see if the local gradient systematically affected the measured K value. It was assumed that the soil permeability was greater than that of the bedrock, and the majority of flow would be lateral rather than vertical, leading to estimates of lateral rather than vertical hydraulic conductivity.

The bedrock hydraulic conductivity was measured during three sprinkling experiments. A 2 m wide line source upslope of the monitoring trench was sprinkled continuously until a steady state flux was achieved at the trench (3 to 5 days). The flux into the bedrock was determined as the difference between the steady state sprinkling flux and the flux into the trench at the bottom of the hillslope. Under the assumption of unit head gradient, the saturated hydraulic conductivity of the bedrock was then calculated through dividing the bedrock flux by the area over which bedrock infiltration occurs (i.e. the product of the width of the line source and the distance between line source and trench).

This approach was repeated for three locations at each of 6 m, 9 m, and 14 m upslope of the trench. For the upslope sections, the loss was determined as the difference between the volume applied, the volume captured in the trench and the measured loss in the section downslope. Losses and derived bedrock hydraulic conductivities were determined for nine 16 m^2 sections of the hillslope (see positions shown in Fig. 1a). Despite high water application rates (0.29 l s^{-1} or approximately 44 mm hr^{-1}), no overland flow was observed.

To analyze the relationship between hydraulic conductivity and the bedrock topography that governs the direction of lateral subsurface flow, we calculated the flow accumulated area and topographic wetness index (TWI) of the bedrock topography. The cell size of the bedrock DEM was small compared to the size of the topographic depressions; hence we used a D8 algorithm to calculate flow accumulation. The topographic wetness index (TWI) was calculated with the following equation (Kirkby, 1975):

$$\mathrm{TWI} = \ln(\alpha/\tan\beta) \quad (4)$$

Where α is the upslope area per unit contour length (m^2 m^{-1}) and β is the local slope gradient (°). The unit contour length was 1 m in this study.

3.2 Model setup

We developed a distributed hydrological model to simulate the spatial distribution of groundwater recharge.

We assumed that all throughfall (the fraction of precipitation that is not intercepted by vegetation) infiltrated into the soil. The throughfall volume was calculated with an empirical formula (eq. 5) determined by Tromp-van Meerveld and McDonnell (2006a) from storm events at PMRW (Cappellato *et al*., 1995).

$$T = 0.97P - 1.66 \quad (5)$$

Where T is the throughfall depth of a rainstorm (mm) and P is the depth of the rainstorm (mm). For potential transpiration rate of the vegetation we used the average daily rate of 2.6 mm d^{-1} measured during the 2002 growing season. In the model simulations, the actual transpiration per timestep from each soil column was determined as the minimum of two volumes:

$$T_{ACT} = \min(T_{POT}, S_{ACT}) \quad (6)$$

Where T_{ACT} is the actual volume of transpiration (m), T_{POT} is the potential volume of transpiration (m), and S_{ACT} is the actual volume of water stored in the soil column (m). We assumed an immediate and uniform distribution of moisture in the soil column. Where there was no soil present, water was immediately added to the soil-bedrock interface reservoir.

The soil was represented by a single column above each bedrock topography cell. We assumed unsaturated flow was a consequence of gravity drainage only (i.e. unit gradient flow) (eq. 7).

$$q_V = -K_{eff} \quad (7)$$

Where q_V is the unsaturated flux (m d^{-1}) and K_{eff} is the effective conductivity (m d^{-1}). The effective hydraulic conductivity (eq. 8) is calculated as a function of the saturated hydraulic conductivity and the relative conductivity.

$$K_{eff} = K_V K_r \quad (8)$$

Where K_V is the saturated hydraulic conductivity of the soil in vertical direction (m d^{-1}) and K_r is the relative conductivity (-), calculated with the van Genuchten-Mualem equation (van Genuchten, 1980):

$$K_r = \sqrt{\frac{\theta_a-\theta_r}{\theta_s-\theta_r}}\left(1-\left(1-\left(\frac{\theta_a-\theta_r}{\theta_s-\theta_r}\right)^{\frac{1}{m}}\right)^{m}\right)^{2} \quad (9)$$

Where θ_a is the actual soil moisture content, θ_s the saturated soil moisture content, and θ_r the residual soil moisture content. The m (-) parameter is related to the shape parameter n (-) from the Van Genuchten water retention curve through:

$$m = 1 - 1/n \quad (10)$$

Groundwater recharge (GWR) was determined as a direct loss from the soil-bedrock interface (SBI) reservoir. If there is water present in this reservoir at any point of the hillslope, the recharge rate, q_{gwr} (m d^{-1}) was determined as the minimum of two rates:

$$q_{gwr} = \min(q_V, K_{BR}) \quad (11)$$

Where q_V is the drainage from the soil (m d^{-1}) and K_{BR} (m d^{-1}) is the saturated hydraulic conductivity of the bedrock. The storage capacity of the bedrock was assumed to be infinite.

When the recharge rate into the bedrock was too small to drain the SBI reservoir during the timestep, water was routed along the SBI topography. The routing algorithm takes into account changes in flow directions caused by filling and spilling of depressions in the microtopography (Appels *et al.*, 2011). We replaced the original instantaneous water transfer in the redistribution algorithm with a kinematic wave approximation of the Boussinesq equation over a sloping boundary (eq. 12, Rupp and Selker (2006)) to account for the spatial variability of horizontal hydraulic conductivity.

$$Q_L = K_L b h \frac{dH}{dx} \tag{12}$$

Where Q_L is the lateral flux of water (m^3 d^{-1}), K_L is the saturated hydraulic conductivity of the soil in lateral direction (m d^{-1}), b is the width of flow (m), h is the height of the saturated layer (m), and dH/dx is the hydraulic head gradient (m m^{-1}), that is assumed to be equal to the gradient of the bedrock surface in the direction of flow. The flow direction along the SBI was determined for every timestep, based on the highest local gradient of the hydraulic head. The resulting flow was then calculated in a single direction (eq. 12).

The height of the saturated zone was transient and assumed to be unrelated to the soil column height, implying the presence of a transient thin soil layer for saturated flow at the locations where the bedrock was exposed. At the domain boundary, water was allowed to drain freely from the seepage face without outflow resistance. The conceptualization of soil and saturated zone above the SBI is illustrated in Fig. 2.

3.3 Generation of fields of hydraulic conductivity

Our model required three spatial distributions of hydraulic conductivity: vertical and lateral direction in the soil and vertical in the bedrock. Spatially variable fields of hydraulic conductivity were generated from the results of a geostatistical analysis of the conductivity measurements. The geostatistical analysis of the measurements was performed with the nlme and geoR packages of R statistical software (Pinheiro *et al.*, 2013; Diggle and Ribeiro, 2007) Based on the best-fitting models for the measurements, as presented in Table 1, random fields were generated with the RandomFields package (Schlather *et al.*, 2014) of R statistical software (R Core Team, 2014). The random field generation was performed with the log10 transformed measurement values due to non-normally distributed values (see results section 4.1).

The K_L dataset was large enough for a reliable estimate of the spatial distribution of the values, the number of measurements of K_V and K_{BR} was smaller and measurements represented a smaller part of the hillslope. This will likely have had consequences for the estimates of nugget and correlation length of the covariance model (Table 1). We decided to work with these estimates in the absence of larger data availability. The choice of covariance model, specifically the ratio between correlation lengths of the K_{BR} pattern versus that of the K_L and/or K_V, affects the simulations in terms of flow length along the SBI. We do not claim that the geostatistics we used in this study are the ‘right’ ones and varying correlation length will surely affect the results. However, performing a full sensitivity analysis with structures of various length fell outside the scope of this study.

Also, K_{BR} was measured at a larger spatial scale than the cell size of the generated spatial distributions of K_{BR}. However, we assumed that the variance of the measurements was equal to the variance of the smaller spatial scale.

3.4 Parameterization and simulation scheme

Model simulations were performed with 25 combinations of randomly generated hydraulic conductivity fields. We established with a jackknife resampling analysis that the standard deviation of the water balance components did not change when considering 20 simulations or more, suggesting that the results of our set of 25 simulations are not biased to a specific combination of hydraulic conductivity patterns.

The soil hydraulic parameters required for the calculation of the relative conductivity (eq. 9) were uniformly distributed (θ_s = 0.45, θ_r = 0.30, n=1.75). These values were based on previous modeling studies (Hopp and McDonnell, 2009; James et al., 2010). The grid cell size of the domain was set at 0.25 m, such that the heterogeneity of the bedrock topography could be distinguished.

We performed three sets of simulations of increasing complexity to address the effects of (1) spatial variability of hydraulic conductivity, (2) storm duration, and (3) transient precipitation on groundwater recharge on the hillslope. Table 1 presents the parameterization scheme of the simulation sets.
The rainfall event of simulation set 1 has been described and modelled before by Burns *et al*. (2001), Freer *et al*. (2002), Hopp *et al*. (2009), and James *et al*. (2010). The rainfall volume was corrected for throughfall (eq. 5), but transpiration was neglected as this event occurred before the growing season.
The first combination of conductivity values in this first simulation set (Table 2) was based on the average of the measured values of soil and bedrock hydraulic conductivity with a relatively small contrast between vertical hydraulic conductivity of the soil and bedrock (simulations a and d). For the second and third combination, the contrast between K_V and K_{BR} was increased by a factor of 10 (simulations b and e) and a factor of 100 (simulations c and f). Initial conditions and spin up period were the same as used by James *et al*. (2010).
The intensity and lag time used in simulation set 2 were the average storm intensity and the average lag time between storms at Panola, calculated from the 147 storm record (Tromp-van Meerveld and McDonnell, 2006a). In these simulations, transpiration was neglected and the rainfall events were treated as effective throughfall events.
The precipitation series of simulation set 3 was corrected for throughfall (eq. 5) and the potential transpiration rate was set at 2.6 mm d^{-1} during the growing season (1 May to 1 October).

4. Results

4.1 Spatial patterns of soil and bedrock saturated hydraulic conductivity

The measured hydraulic conductivity values of the three zones showed a large variability (Fig. 3 and Table 3). The K_V profiles measured with the Guelph permeameter showed a general tendency of decreasing variability of hydraulic conductivity with depth. However, large values were found at 45 and 72 cm depth (Fig. 3). These may be attributed to the presence of macropores or other vertical preferential flow paths in the soil as identified as important transport mechanisms by Freer *et al*.

(2002). We did not find a statistically significant relation between soil depth and saturated hydraulic conductivity, neither in the vertical nor in the lateral direction.

The ranges of the measured values of saturated hydraulic conductivity of the soil and bedrock overlapped. A Kolmogorov-Smirnov test showed that the lateral saturated hydraulic conductivity (K_L) of the soil was significantly larger than the vertical saturated hydraulic conductivity of the soil (K_V) and the bedrock (K_{BR}), but there was no significant difference between the datasets of K_V and K_{BR} at a *p*-value of 0.10. The size of the K_L values could also have been affected by the local slope of the SBI, reflecting differences in hydraulic head instead of variability of K_L. An analysis of measured K_L values, grouped by soil depth, versus slopes determined from the bedrock DEM did not reveal a correlation between saturated hydraulic conductivity and local slope. In addition, Fig. 4a and 4b show no meaningful correlations of measured K_L values and flow accumulation or topographic wetness index (TWI) based on the bedrock DEM.

Geostatistical analysis of the data showed that a lognormal distribution fitted the observed spatial clustering of hydraulic conductivity better than a normal distribution. An exponential covariance model provided the best fit to all three datasets (Table 3). The coefficient of variation of measured hydraulic conductivity of both K_V and K_{BR} was larger than that of K_L. The correlation length of the fitted covariance models was shortest for the soil hydraulic conductivity in the vertical direction.

4.2 Effects of uniform and spatially variable hydraulic conductivity

In the simulations with uniform parameters (Figs. 5a, b, c) only soil depth and bedrock topography control the spatial pattern of GWR that results after a rainstorm. When the contrast between K_V and K_{BR} was small (Fig. 5a), q_V from the soil exceeded K_{BR} only at locations with soil depths smaller than 0.05 m and lateral flow along the soil-bedrock interface did not extend further than 1 m before reinfiltration. Shallow soil zones were more saturated than deep soil zones and therefore higher amounts of GWR occurred in these zones during the course of the storm. In the uniform simulations with a larger contrast between K_V and K_{BR} (Fig. 5 b and c), q_V from the soil exceeded the K_{BR} early on in the rainstorm and as a result zones with shallow soils now generated lateral flow along the SBI. Zones of high flow accumulation and depression storage in the bedrock topography developed a larger transient saturated layer that provided high GWR in the drainage phase after the storm. Due to the formulation of the q_L in one direction and the lack of detailed topography of the bedrock, the lateral flowpaths along the SBI appear as ribbons of increased GWR in the final maps.

Though the cumulative bedrock groundwater recharge did not exceed the event precipitation at the hillslope scale, local values of groundwater recharge could be much higher as a result of lateral flow and slow recharge from the stagnating saturated layer after the storm: up to a factor three for the uniform conductivity fields and a factor five for the spatially variable conductivity fields.

In the simulations with spatially variable values of K_V, K_L, and K_{BR}, we found that firstly the rate at which water was delivered to the SBI was affected: some deeper soil zones now received more GWR than others in the low-contrast simulation (Fig. 5d). Secondly, the spatial distribution of K_L created a more varied pattern of lateral flow. So while the GWR ribbons were still visible in Figs. 5e and 5f, the GWR pattern surrounding these hotspots of GWR was less smooth.

The low contrast parameter set underestimated subsurface flow at the bottom of the domain most: no flow in the uniform scenario and only 0.05 m^3 cumulative in the spatially variable version. The higher contrast parameter sets all generated significant subsurface flow with a first peak already occurring during the first rain period of the storm. This was an artefact of the model structure that just considered one soil layer and therefore simulated a fast movement of the infiltration front. The spatial distribution of K_V partly mitigated this artefact, because it caused a slight delay of the first runoff peak and a more prolonged drainage phase of the hydrographs after the storm (Figs. 5e and 5f). Simulations c and f resulted in cumulative runoff volumes closest to the observed total runoff of 13.5 m^3, suggesting that this conductivity contrast approaches reality best.

4.3 Effects of storm duration

Fig. 5 showed a clear negative relationship between soil depth and groundwater recharge when hydraulic conductivities were uniformly distributed; the pattern became more varied with spatially variable fields of K. In Fig. 6, the variation of the GWR pattern is explored as a function of storm duration. The coefficient of variation (CV) was determined for all cells that fell within the same soil depth range. The lines in each panel show that though there were considerable differences between the individual combinations of fields (a result of K_V variability), they all display a similar increasing variability as a function of storm duration. In shallower soil classes the range of CV (i.e. the bandwidth of the lines in Fig. 6) increased due to effects of K_{BR} variability: the flux from the soil columns was larger than the flux into the bedrock. In the deeper soil classes the range of CV increased more slowly, because the soil did not reach similar levels of saturation. Increased CV could be attributed to run-on from shallower soil zones.

In all the scenarios, the total amount of rain applied was the same and so was the total amount of groundwater recharge. However, the fraction of total recharge occurring during the storms increased disproportionally with the size of an individual storm event from 7% in the 1-hour storms to 78% in the 20-hour storm. In accordance with this increase, the spatial variability of GWR increased with an increase of storm duration (moving from top to bottom in Fig. 6). In hillslope areas with a soil depth shallower than the critical depth that variability was caused by the spatial distribution of KBR. In hillslope areas with deeper soil depths that variability increased due to increased differences in wetness and induced vertical flux during the storms and run-on from shallow soil depth zones.

The extent of lateral flow can be illustrated by comparing the actual saturated SBI area with the area where SBI was generated because q_V was larger than K_{BR}. Fig. 7 illustrates the increasing extent of run-on with increasing storm duration. The loops in the panels are hysteretic: the saturated area increases during the storm and then sustains saturation during the drainage phase both because percolation rates from wet shallow soil zones are still high and because drainage from the saturated layer continues after the storm. Longer storms resulted in a larger saturated SBI area and more deviation from the 1:1 line, indicating a larger travel distance of lateral flow. The differences between the loops of the individual combinations of K fields show that the exact size and position of the run-on affected areas depends on the particular realization of K_L and K_{BR} fields.

4.4 Analyzing the groundwater recharge pattern – annual precipitation dynamics

The spatial patterns of soil and bedrock conductivity mainly affected yearly cumulatives of subsurface runoff and storage change in the transient saturated layer at the SBI, as indicated in Table 3 by the high coefficients of variation for these water balance components. Since throughfall solely depended on precipitation characteristics, this volume was identical for all simulations.

Figure 8 shows the empirical cumulative distribution function of groundwater recharge and cumulative rainfall as a function of event throughfall. Events were defined as the duration of the rainstorm and 24 dry hours after a storm. Our simulations showed that 25% of annual groundwater recharge occurred during events with 9.7 mm throughfall or less, 50% of annual GWR during events with throughfall of 37 mm or less, and 75% of annual GWR during events with throughfall of 84 mm or less (Fig. 8). A total of 40% of annual groundwater recharge occurred during events that exceeded the precipitation threshold for subsurface flow of 52 mm throughfall (Tromp-van Meerveld and McDonnell, 2006a). Groundwater recharge under saturated areas accounted for 40% of the annual total GWR.

Maps of cumulative GWR during various periods of the simulation and of different realizations of *K* fields are shown in Fig. 9. These maps show that GWR hotspots (in red) changed with storm magnitude. In a lag period (Fig. 9a), the zones with deep soil depth received the largest amounts of GWR, whereas in an event period with the same average amount of groundwater recharge (Fig. 9b) more recharge occurred in zones with a shallow soil. Events needed to be of a considerable size to have increased GWR occur along lines of higher flow accumulation (Fig. 9d). The relative contribution of GWR hotspots to the total volume varied per event between 12 and 90%, depending on the extent of lateral flow. On a yearly timescale (Fig. 10), the hotspots received 30% of the bedrock groundwater recharge.

When the yearly cumulative groundwater recharge at each point of the hillslope was plotted as a function of the duration of saturation at the soil-bedrock interface (Fig. 10), three zones could be distinguished: 1) a zone without a strong correlation between duration of saturation and amount of GWR, 2) a zone where long durations of saturation corresponded to high yearly GWR, 3) a zone displaying the same correlation, but at a steeper slope.

5 Discussion

5.1 A perceptual model of the spatial hierarchy of groundwater recharge at the hillslope scale

Our simulations suggest that the relative importance of each of the structural and dynamic controls on groundwater recharge into bedrock at the hillslope scale varies with rainstorm size and the duration of dry periods between events. The structural aspects of the hillslope include its bedrock topography, soil depth, soil hydraulic properties - characteristics that are assumed to be constant on the recharge timescale. The dynamic aspects include the rate at which water is delivered to, and the extent to which lateral flow is present at, the soil-bedrock interface – characteristics that are transient on the recharge timescale.

Dynamic aspects drive the hierarchy of controls, expressed as a flow chart in Fig. 11. Firstly, the ratio between rain depth (ΣP) and soil water storage capacity (V_{soil}) determines the size of the vertical flux of water through the soil. Secondly, the ratio between this vertical flux (q_V) and the flux into the bedrock (q_{gwr}) determines the level of saturation at the soil-bedrock interface (SBI). Thirdly, the ratio between the lateral flux (q_L) from saturated areas at the soil-bedrock interface and the flux into the bedrock (q_{gwr}) determines the run-on distances along the SBI. When the first and second ratio are small, the spatial pattern will reflect the spatial distribution of soil depth. Conversely, when widespread SBI saturation occurs, run-on distances are large and increased GWR will occur within zones of high flow accumulation and depression storage in the bedrock topography (SBI_{topo}). The transition phase between soil depth and topography controlled recharge occur under lower soil-bedrock interface saturation, when the K_L patterns on the hillslope control run-on distances and resulting increased bedrock groundwater recharge. This is an example of structural hillslope characteristics influencing a dynamic control.

We found that the spatial variability of soil depth trumped the spatial variability of K_V as an influential factor, because the spatial variability of the delivery rate was mainly determined by the soil moisture content. Shallow soil zones not only delivered more water to the soil-bedrock interface, but also at a higher rate, because they reach a state of higher saturation than their deeper soil counterparts during average rainstorms. The spatial variability of K_V played a smaller role, but affects the variation around the groundwater recharge-soil depth relationship

The presence of fractures or another type of variety of bedrock permeability is a structural aspect for increased bedrock groundwater recharge potential (as opposed to an average value of bedrock permeability as estimated by Tromp-van Meerveld *et al*., 2007). Fractures will act as hot spots for groundwater recharge, due to their large potential loss rate. Though our model does not explicitly account for fracture flow, the randomly generated fields of K_{BR} contained points with values large enough to be considered as fractures. Our results show that the combined vertical and lateral flux is not always large enough for the actual loss rate to equal the potential loss rate. Instead, increased bedrock groundwater recharge will also occur at locations with smaller K_{BR}, but with accompanying prolonged saturation at the soil-bedrock interface. In general, lateral flow ceases within 24 hours after rainfall events and the saturated layer is drained by vertical recharge into the bedrock. Recharge from this saturated layer occurs faster than drainage from the soil and is the main reason why the fraction of recharge occurring during rain storms increases non-linearly with storm size.

The storm throughfall amount determined the extent over which saturation at and lateral flow along the SBI occurred. Lateral flow occurred during virtually all rainfall events in this conceptual model, but it did not always reach further than cells directly neighboring locations where it was generated. Therefore, the timescale over which we made the groundwater recharge and the selection of an event or lag period determined the spatial pattern of the GWR maps.

In our simulations, high flow accumulation zones were the main control on GWR patterns during rainstorms larger than 50 mm throughfall or smaller storms on a very wet (>60% saturation) soil. This 50 mm is fairly consistent with the 52 mm throughfall threshold for subsurface flow at Panola as found by Tromp-van Meerveld and McDonnell (2006b).
In the hydrological year we investigated 10% of the annual throughfall occurred in events larger than that threshold. These events provided 40% of the simulated annual groundwater recharge. On an annual basis, 23% of simulated GWR occurred in the lags between storms, during which soil depth is the main control on the GWR pattern. The remaining 33% of GWR occurred in ‘transition phase’ rainstorms, with relatively short run-on distances. In this transition phase, sections of the hillslope are in different stages of the hierarchy in Fig. 11 during the same event.

Consistent with Hopp and McDonnell (2009) and Harman and Sivapalan (2009) the average soil depth, bedrock permeability, soil hydraulic conductivity and lower boundary conditions determine the hillslope integrated water balance. However, individual spatial distributions of these hillslope characteristics strongly determine the spatial pattern of bedrock groundwater recharge hotspots. When defined as locations with groundwater recharge greater than the 90-percentile value, 30% of annual GWR occurs in hotspots (i.e. 10% of the hillslope area receives 30% of the hillslope recharge). However, the contribution and the position of hotspots depends on the timescale that is chosen to analyze GWR and also between events, depending on the presence and extent of lateral flow at the soil-bedrock interface.
Our perceptual model of bedrock groundwater recharge illustrates that the dynamic aspects driving the spatial pattern of bedrock groundwater recharge, i.e. rainstorm size in proportion to soil water storage capacity, are key factors in the occurrence and positioning of recharge hotspots. Our perceptual model of groundwater recharge occurring at short distances downslope of the original point of infiltration of throughfall fits well into the interflow framework proposed by Jackson *et al*. (2014). It accounts for saturated zones developing in a fragmented fashion along the hillslope, converging along lines of flow accumulation when storms are large. This model is consistent with the fill-and-spill of bedrock topography in the sense that in order to generate subsurface stormflow at the lower boundary of the hillslope, the fill zones need to be fully saturated and connected. However, these zones do not map one to one to hotspots of groundwater recharge, due to the heterogeneity that is created by short distance run-on during events below the threshold.

5.2 On groundwater recharge and measurement scale

We caution that the results presented in this paper are simulation results. The overlap of simulated patches of transient saturation at the soil-bedrock interface with increased groundwater recharge was promising, but we cannot evaluate our model with measured values of bedrock groundwater recharge at the site— a notoriously difficult measurement to make (Shand *et al.*, 2005; Heppner *et al.*, 2007;

Gleeson *et al.*, 2009; Salve *et al.*, 2012). That said, experimental studies at other hillslope sites have reported both the distinctive slow, widespread recharge during dry periods versus fast, localized recharge in wet periods (Anderson *et al.*, 1997; Gleeson *et al.*, 2009) and large differences in magnitude of response in individual wells to events (Salve *et al.*, 2012).

In this study, we have shown how spatially variable distributions of conductivity play a role in creating a recharge flux that is highly variable in space and time. We combined two sets of point-scale measurements (Guelph permeameter and well-based falling head measurements) with more integrated measurements (sprinkling experiment) to generate spatial distributions of conductivity on our hillslope. We worked from the premise that these experiments provided a range of values of soil and bedrock conductivity and a first quantitative measure of their spatial correlation; but not a set of exact values at each point of the hillslope.

The sprinkling experiments at various sections of the hillslope above the trench showed a large range of K_{BR} variability (consistent with the sprinkling experiment performed by Tromp-van Meerveld *et al*. (2007)), even though the section areas were still rather large and individual fractures were not mapped or instrumented. In order to estimate the actual locations of increased bedrock recharge (e.g. everything higher than the 90-percentile value as per Fig. 10), quantifying the local extent of lateral flow along the soil-bedrock interface is an important step. Our work suggests that due to the higher frequency of small rainstorms and the resulting occurrence of lateral flow over short distances at the site, the spatial distribution of K_L was as important as that of K_{BR}. The well-based falling head experiment, as simplistic as it was, provided some insights into that distribution. The experimental method had some drawbacks: (1) the direction of flow was not well defined (saturation around the wells most likely occurred as a "bulb" of wetting) and (2) it was a combined measurement of soil and bedrock permeability so that neither could be individually resolved. The latter is not an issue if the contrast between soil and bedrock permeability is high. Notwithstanding these issues, one of the interesting measurement results was that these ranges of conductivity overlap. This may imply that local conductivity contrasts are smaller than generally acknowledged at the site until now (compare the high average contrast calculated by Tromp-van Meerveld *et al*., 2007). It may further imply that some of the well-based falling head measurements were measuring the conductivity of the bedrock and not that of the soil. Since the soil consists of colluvium originating from upslope parent material, it is perhaps not surprising that the saturated hydraulic conductivity of soil and bedrock were not spatially correlated. However, given the occurrence of subsurface flow on the site, we expected that K_L above the SBI would be related to topographic characteristics of the bedrock that govern lateral flow. Where lateral flow accumulates, more weathering could result in eroded soil pipes or, conversely, clogging due to flushing and accumulation of fine materials. Hence, we expected a correlation of K_L with flow accumulation or topographic wetness index (TWI). The lack of such a correlation (Fig. 4) illustrates the need of separate spatial surveys of conductivity at other sites instead of using bedrock topography or soil depth as a proxy for the distribution of K_L.

A logical follow up would be a detailed survey of distributions of hydraulic conductivity at a site such as Rivendell (Salve *et al.*, 2012; Kim *et al.*, 2014) to see if these can be used to explain the lack of uniformly rising and falling perched groundwater table at the site. It is intuitive to focus measurement campaigns on large events that feature subsurface runoff at the toe of a hillslope, but for improving our understanding of spatial variability of groundwater recharge more emphasis should be put on measuring flow distances during smaller events.

5.3 On the value of a simple modeling approach

The results of this study show that the location of hotspots of bedrock groundwater recharge is determined largely by the spatial distribution of lateral soil hydraulic conductivity, bedrock hydraulic conductivity and the extent of lateral flow that is generated on the hillslope during a multi-storm timeseries.

The first weakness of our modeling approach is that we do not simulate flow through the bedrock matrix and fractures. The unlimited unit gradient flux into the bedrock likely overestimates recharge under unsaturated drainage conditions and underestimates such fluxes during periods of transient saturation at the soil-bedrock interface. Also, we did not simulate return flow from upslope fractures into the soil further downslope and thus ignore feedbacks between bedrock and soil as for instance observed by Montgomery *et al.* (1997) and Shand *et al.* (2007). Secondly, we restricted lateral flow to the soil-bedrock interface, where a more sophisticated physical model could simulate perched groundwater flow. The rationale for the assumption of restricted lateral flow is found in previous field and modeling studies at the site that have shown that saturated flow mainly occurs at this interface.

The lack of bedrock flow simulation is more difficult to defend as we do not have data to support our modeling choices. The shallow bedrock geology of the hillslope likely contains connected fractures parallel to the land surface since it is constructed from granite blocks (Tromp-van Meerveld *et al*., 2007). Connected fractures in the bedrock may produce return flow from the bedrock into the hillslope, but there is no experimental evidence confirming or negating this. Previous modeling studies of the Panola hillslope by Hopp and McDonnell (2009) and James *et al*. (2010) contained hydrologically active bedrock, but did not consider fracture flow either.

Incorporating both the spatial variability of saturated hydraulic conductivity of soil and bedrock, and bedrock topography on a hillslope while running a model that deals with matrix and fracture flow remains a computational challenge. Modeling studies of similar hydrogeological systems with more sophisticated numerical tools (e.g. HydroGeoSphere by Gleeson *et al*., 2009) are therefore necessarily restricted to a simpler description of their modeling domain. In a recent study with a 3D Richards' solver by Liang and Uchida (2014), soil depth and TWI were found to be first-order controls on transient saturation at the SBI in a steep catchment with a high intensity rainstorm. As shown in this study, this is an extreme scenario; on gentle hillslopes and during shorter rain events local flow heterogeneities are likely more important controls. Alternatively, instead of using more powerful Darcy-Richards solvers for this type of problem that feature non-Darcian flow in both soil and bedrock, different conceptual approaches to fast recharge such as the one proposed by Mirus and Nimmo (2013) may be a successful way forward.

6. Conclusions

We examined the spatiotemporal distribution of bedrock groundwater recharge at the hillslope scale at the well-studied Panola experimental hillslope. We used new measurements of spatially variable soil and bedrock hydraulic conductivity and a multi-event precipitation series to perform simulations of groundwater recharge with a new, simple, spatially distributed model.

We found that the major part of simulated groundwater recharge during a hydrological year occurred under unsaturated drainage. Soil depth was a main control on amounts and rates through available storage capacity and controlling the size of vertical flux. During rain storms transient saturation occurred at the soil-bedrock interface and lateral flow started to affect groundwater recharge patterns. There were two aspects to that: firstly, hillslope SBI locations that received more lateral flow and had increased saturation at the end of a storm received more groundwater recharge. Secondly, increased lateral flow transported water to locations where the bedrock permeability was higher.
We have shown that under the rainfall regime found at Panola and the specific distribution of soil and bedrock hydraulic properties, hillslope-wide SBI saturation only occurred during extreme rainfall events. While these contributed a large amount of water, the main controls on an annual scale were therefore not just soil depth and bedrock topography, i.e. the factors that control fill and spill areas in the subsurface. Instead, hydraulic conductivity, both that of bedrock and the 'lateral' soil, determined the activation and extent of lateral flow along the SBI.

The results of this study highlight the importance of 3D modeling and simulation of multi-storm time series when investigating groundwater recharge distributions. Point-scale modeling by definition underestimates the variability of the process and cannot account for variation in location and timing of increased bedrock groundwater recharge as does modeling at the watershed scale. This is in accordance with results of subsurface stormflow studies. We propose that in order to improve our understanding of the spatiotemporal dynamics of groundwater recharge at the hillslope scale, we go back to subsurface runoff hillslopes and try to quantify the characterizing ratios between delivery and loss rate and rain storm size and extent of lateral flow.

7. References

Allison. G. , G. Gee, and S. Tyler. 1994. Vadose-Zone Techniques for Estimating Groundwater Recharge in Arid and Semiarid Regions. *Soil Science Society of America Journal*, **58**(1), 6–14.

Appels, W.M., P. W. Bogaart, and S. E. A. T. M. van der Zee. 2011. Influence of spatial variations of microtopography and infiltration on surface runoff and field scale hydrological connectivity. *Advances in Water Resources*, **34**(2), 303–313.

Asano, Y., T. Uchida, and N. Ohte. 2002. Residence times and flow paths of water in steep unchannelled catchments, Tanakami, Japan. *Journal of Hydrology*.,**261**(1–4), 173–192.

Bachmair, S., and M. Weiler, 2011. New Dimensions of Hillslope Hydrology. In: *Forest Hydrology and Biogeochemistry.Synthesis of Past Research and Future Directions*, D.F. Levia *et al*. (eds), 455–481, Springer, Netherlands.

Barron, O.V., R. S. Crosbie, W. R. Dawes, S. P. Charles, T. Pickett, and M. J. Donn. 2012. Climatic controls on diffuse groundwater recharge across Australia. *Hydrology and Earth System Science*, **16**(12), 4557–4570.

Burns, D. A., J.J. McDonnell, R. P. Hooper, N.E. Peters, J.E. Freer, C. Kendall and K. Beven (2001). Quantifying Contributions to Storm Runoff through End-Member Mixing Analysis and Hydrologic Measurements at the Panola Mountain Research Watershed (Georgia, USA). *Hydrological Processes*, **15**(10): 1903-1924.

Buttle, J.M. and D. J. McDonald. 2002. Coupled vertical and lateral preferential flow on a forested slope. *Water Resources Research*, **38**(5), 1060.

Cappellato, R. and N. Peters. 1995. Dry Deposition and Canopy Leaching Rates in Deciduous and Coniferous Forests of the Georgia Piedmont - an Assessment of a Regression-Model. *Journal of Hydrology*, **169**(1–4), 131–150.

De Vries, J. and I. Simmers. 2002. Groundwater recharge: an overview of processes and challenges. *Hydrogeology Journal*, **10**(1), 5-17. DOI:10.1007/s10040-001-0171-7

Diggle, P.J. and P. J. Ribeiro. 2007. Model-based Geostatistics. Springer, New York.

Ebel, B.A. and K. Loague. 2008. Rapid simulated hydrologic response within the variably saturated near surface. *Hydrological Processes*, **22**(3), 464–471.

Ebel, B.A., and J.R. Nimmo. 2013. An Alternative Process Model of Preferential Contaminant Travel Times in the Unsaturated Zone: Application to Rainier Mesa and Shoshone Mountain, Nevada. *Environmental Modeling & Assessment*, **18**(3): 345–63. doi:10.1007/s10666-012-9349-8.

Flint, L.E., A. L. Flint, B. J. Stolp, and W. R. Danskin. 2012. A basin-scale approach for assessing water resources in a semiarid environment: San Diego region, California and Mexico. *Hydrology and Earth System Sciences*, **16**(10), 3817–3833.

Freer, J., J.J. McDonnell, D. Brammer, K. Beven, R. Hooper, D. Burns (1997). Topographic controls on subsurface stormflow at the hillslope scale for two hydrologically distinct catchments. *Hydrological Processes*, **11**(9): 1347-1352.

Freer, J., J.J. McDonnell, K. J. Beven, N. E. Peters, D. A. Burns, R. P. Hooper, B. Aulenbach, and C. Kendall. 2002. The role of bedrock topography on subsurface storm flow. *Water Resources Research*, **38**(12): 5-1 - 5-16.

Gabrielli, C., J.J. McDonnell and T. Jarvis, 2012. The role of bedrock groundwater in rainfall-runoff response at hillslope and catchment scales. *Journal of Hydrology* **450-451**: 117-133.

Gleeson, T., K. Novakowski, and T. K. Kyser. 2009. Extremely rapid and localized recharge to a fractured rock aquifer. *Journal of Hydrology*, **376**(3–4), 496–509.

Graham, C., H. Barnard, W. van Verseveld and J. J. McDonnell. 2010. Estimating the deep seepage component of the hillslope and catchment water balance within a measurement uncertainty framework. *Hydrological Processes*, DOI: 10.1002/hyp.7788.

Harman, C., and M. Sivapalan. 2009. Effects of Hydraulic Conductivity Variability on Hillslope-Scale Shallow Subsurface Flow Response and Storage-Discharge Relations. *Water Resources Research* **45**.

Hebert, G. 2005. A Geophysical Investigation of Hydraulic Pathways at the Panola Mountain Research Watershed. MSc thesis. Georgia Institute of Technology. http://hdl.handle.net/1853/7484

Heppner, C.S., J. R. Nimmo, G. J. Folmar, W. J. Gburek, and D. W. Risser. 2007. Multiple-methods investigation of recharge at a humid-region fractured rock site, Pennsylvania, USA. *Hydrogeology Journal*, **15**(5), 915–927.

Hopp, L. and J.J. McDonnell. 2009. Connectivity at the hillslope scale: Identifying interactions between storm size, bedrock permeability, slope angle and soil depth. *Journal of Hydrology*, **376**, 378-391, DOI: 10.1016/j.jhydrol.2009.07.047.

Jackson, C.R., M. Bitew, and E. Du. 2014. When interflow also percolates: downslope travel distances and hillslope process zones. *Hydrological Processes*, **28**(7), 3195–3200.

James, A., J.J. McDonnell, Ilja Tromp van Meerveld, and Norman E. Peters. 2010. Gypsies in the palace: Experimentalist's view on the use of 3-D physics based simulation of hillslope hydrological response. *Hydrological Processes*, **24**, 3878-3893 (2010) DOI: 10.1002/hyp.7819.

Kirkby, M. 1975. Hydrograph modelling strategies. In: *Processes in Physical and Human Geography*, R. Peel *et al*. (eds), 69– 90, Heinemann, London.

Liang, W.L., and T. Uchida. 2014. Effects of topography and soil depth on saturated-zone dynamics in steep hillslopes explored using the three-dimensional Richards' equation. *Journal of Hydrology*, **510**, 124–136.

Mair, A., B. Hagedorn, S. Tillery, A. I. El-Kadi, S. Westenbroek, K. Ha, and G.-W. Koh. 2013. Temporal and spatial variability of groundwater recharge on Jeju Island, Korea. *Journal of Hydrology*, **501**, 213–226.

McDonnell, J.J., 2013. Are all runoff processes the same? *Hydrological Processes*, **27**(26), 4103-4111. DOI: 10.1002/hyp.10076.

Mirus, B.B. and J. R. Nimmo. 2013. Balancing practicality and hydrologic realism: A parsimonious approach for simulating rapid groundwater recharge via unsaturated-zone preferential flow. *Water Resources Research*, **49**(3), 1458–1465.

Montgomery, D.R. and W. E. Dietrich. 2002. Runoff generation in a steep, soil-mantled landscape. *Water Resources Research*, **38**(9), 1168.

Pangle, L.A., J.W. Gregg and J.J. McDonnell. 2014. Rainfall seasonality and an ecohydrological feedback offset the potential impact of climate warming on evapotranspiration and recharge. *Water Resources Research*, **50**(2), 1308-1321. DOI: 10.1002/2012WR013253

Pinheiro, J., D. Bates, S. DebRoy, D. Sarkar, and R Development Core Team. 2013. nlme: Linear and Nonlinear Mixed Effects Models.

R Core Team. 2014. R: A language and environment for statistical computing. R Foundation for Statistical Computing, Vienna, Austria, 2014.

Scanlon, B.R., R. W. Healy, and P. G. Cook. 2002. Choosing appropriate techniques for quantifying groundwater recharge. *Hydrogeology Journal*, **10**(1), 18–39.

Schlather, M., A. Malinowski, M. Oesting, D. Boecker, K. Strokorb, S. Engelke, J. Martini, P. Menck, S. Gross, K. Burmeister, J. Manitz, R. Singleton, B. Pfaff, and R Core Team. 2014. RandomFields: Simulation and Analysis of Random Fields.

Torres, R. W.E. Dietrich, D.R. Montgomery, S.P. Anderson, and K. Loague. 1998. Unsaturated zone processes and the hydrologic response of a steep, unchanneled catchment. *Water Resources Research*, **34** (8), 1865-1879, DOI: 10.1029/98WR01140.

Troch, P.A., A. Berne, P. Bogaart, C. Harman, A. G. J. Hilberts, S. W. Lyon, C. Paniconi, V. R. N. Pauwels, D. E. Rupp, J. S. Selker, A. J. Teuling, R. Uijlenhoet, and N. E. C. Verhoest. 2013. The importance of hydraulic groundwater theory in catchment hydrology: The legacy of Wilfried Brutsaert and Jean-Yves Parlange. *Water Resources Research*, **49**(9), 5099–5116.

Tromp Van Meerveld, I. and J.J. McDonnell. 2006a. “Threshold relations in subsurface stormflow 1: A 147 storm analysis of the Panola hillslope trench”. *Water Resources Research*, **42**, doi:10.1029/2004WR003778.

Tromp-van Meerveld, H.J. and J.J. McDonnell. 2006b. “Threshold relations in subsurface stormflow 2: The fill and spill hypothesis: an explanation for observed threshold behavior in subsurface stormflow”. *Water Resources Research*, **42**, doi:10.1029/2004WR003800.

Tromp-van Meerveld, H.J. and J.J. McDonnell. 2006c. On the interactions between the spatial patterns of topography, soil moisture, transpiration and species distribution at the hillslope scale. *Advances in Water Resources*, **29**, 293-310.

Tromp van Meerveld, H.J. and J.J. McDonnell. 2007. Effect of bedrock permeability on subsurface stormflow and the water balance of a trenched hillslope at the Panola Mountain Research Watershed, Georgia, USA. *Hydrologic Processes*. **21**, 750-769.

Tromp van Meerveld, H.J. and J.J. McDonnell 2009. On the use of multi-frequency electromagnetic induction for the determination of temporal and spatial patterns of hillslope soil moisture. *Journal of Hydrology*, **368**(1), 56-67.

van Genuchten, M.Th. 1980. A closed-from equation for predicting the hydraulic conductivity of unsaturated soils. *Soil Science Society of America Journal*, **44**, 892-898.

White, A.F., T. D. Bullen, M. S. Schulz, A. E. Blum, T. G. Huntington, and N. E. Peters. 2001. Differential rates of feldspar weathering in granitic regoliths. *Geochimica et Cosmochimica Acta*, **65**(6), 847–869.

White A.F., A. E. Blum, M. S. Schulz, T. G. Huntington, N. E. Peters, and D. A. Stonestrom, 2002. Chemical weathering of the Panola Granite: Solute and regolith elemental fluxes and the weathering range of biotite. In: *Water-Rock Interactions, Ore Deposits, and Environmental Geochemistry: A Tribute to David A. Crerar.* R. Hellmann, S.A. Wood (eds), **7**, 37–59.

Table 1. Overview of setup of the simulations.

	Simulation scheme – Effect of:		
	1. Uniform and spatial variability of hydraulic conductivity	2. Storm duration	3. Transient precipitation
K_V, K_L, K_{BR}	3 realizations of spatially variable K and 3 realizations of spatially uniform K. Values presented in Table 2.	25 realizations of spatially variable K generated with geostatistics presented in Table 3.	25 realizations of spatially variable K generated with geostatistics presented in Table 3.
Forcing	A single long rainfall event that occurred on 6 and 7 March 1996, during which 87 mm of rain precipitated following a dry period of seven days.	100 mm rain precipitated at a rate of 5 mm hr^{-1} in 1, 2, 5, 10, or 20 rainfall events. Each event is followed by a 4.5 day dry spell.	A full year of precipitation, measured in 1997.
Initial condition	$\theta_i = 0.375$	$\theta_i = 0.38$ and $\theta_i = 0.32$	$\theta_i = 0.38$

Table 2. Saturated hydraulic conductivity values used in the simulations presented in Fig. 5. Simulations a-c were parameterized with the mean values of the spatially variable fields of simulations d-f.

	Spatially uniform	Spatially variable	Soil vertical (K_V) (cm hr^{-1})	Soil lateral (K_L) (cm hr^{-1})	Bedrock (K_{BR}) (cm hr^{-1})
Simulation	a	d	2.5	67	0.83
	b	e	2.5	67	0.083
	c	f	25	67	0.083

Table 3. Statistics of saturated hydraulic conductivity of the soil and bedrock.

	Measured (log10 transformed values of cm hr^{-1})			Fitted exponential covariance model (log10 transformed values of cm hr^{-1})			
	Mean	Variance	Min-Max range	Mean	Variance	Nugget	Correlation length (m)
Soil vertical (K_V)	-0.17	0.34	-1.2 – 1.3	-0.05	0.59	0.0	15.6
Soil lateral (K_L)	1.5	0.36	-1.1 – 2.3	1.5	0.38	0.26	20.6
Bedrock (K_{BR})	-0.11	0.078	-0.64 – 0.21	-0.11	0.078	0.0	30.5

Table 4. Water balance components of full year simulation mean (standard deviation) of the 25 random realization combinations.

	Throughfall	Transpiration	Groundwater recharge	Runoff	Storage change unsaturated soil	Storage change saturated layer
Yearly mean and standard deviation (m^3)	1800 (0)	419 (0.7)	1337 (7)	47 (7)	-7.2 (1)	4.2 (3)
Percentage of yearly throughfall (%)	100	23	74	2.6	-0.4	0.2

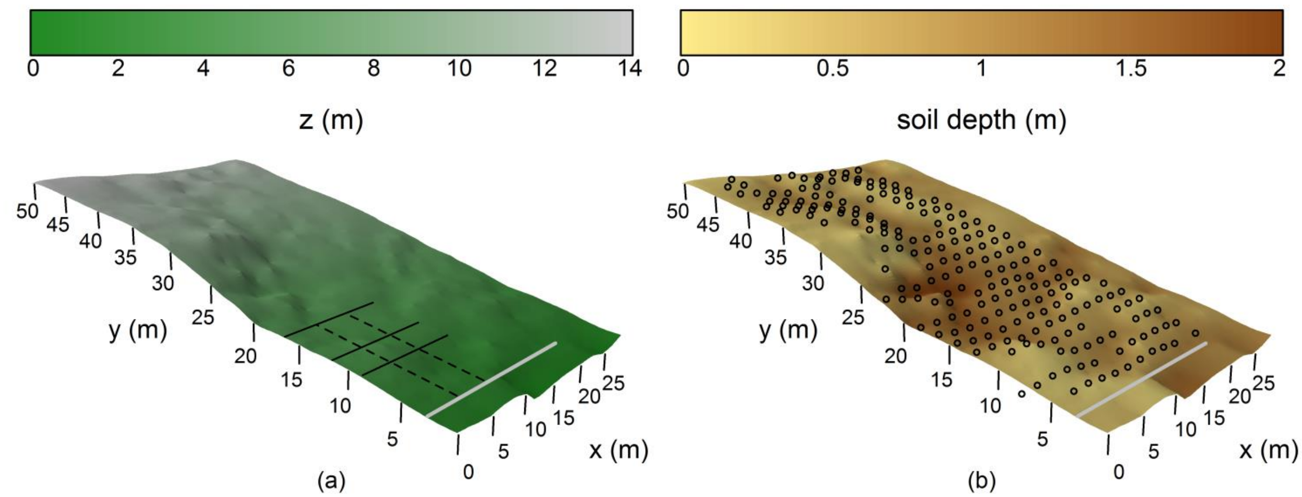

Fig. 1. (a) Bedrock topography of the Panola hillslope, interpolated to a 0.25x0.25 m grid. The grey line indicates the position of the trench. The black solid lines indicate the position of the sprinkling lines, the dashed lines indicate the projected trench sections for which bedrock losses could be determined (b) Soil depth distribution of the Panola hillslope, interpolated to a 0.25x0.25 m grid. The circles indicate the location of the wells (piezometers). The grey line indicates the position of the trench. The actual values of hydraulic conductivity are shown in Fig. 2 and Table 1.

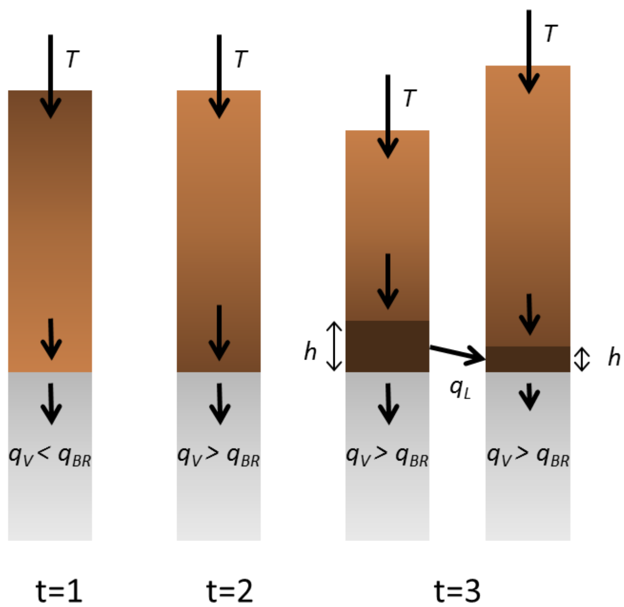

Fig. 2. Illustration of the subsurface conceptualization at three subsequent timesteps during a rainstorm. At t=1, the soil is still unsaturated and the vertical flux from the soil is smaller than the maximum K_{BR}. Due to the wetting of the soil column at t=2, the vertical flux from the soil is now larger than the flux into the bedrock and a saturated layer starts to form at the soil-bedrock interface. At t=3, water in the saturated layer moves laterally from one column to its neighboring soil column.

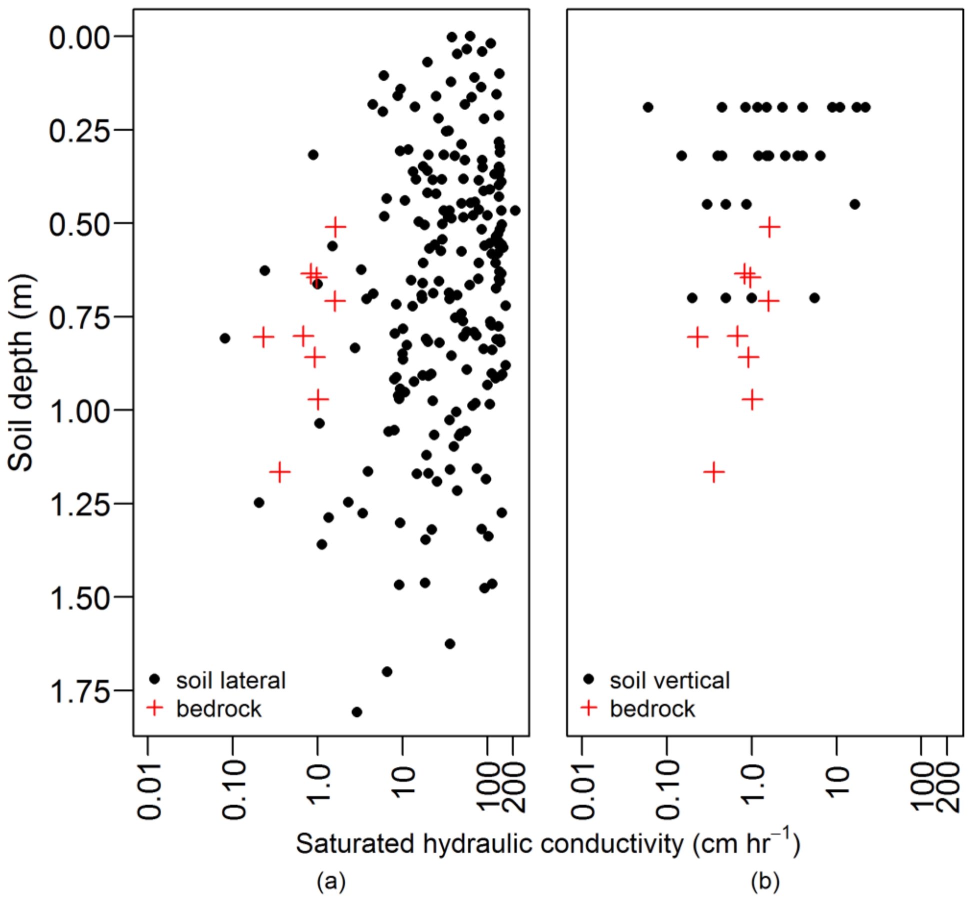

Fig. 3. Measured values of saturated hydraulic conductivity plotted against soil depth: a) conductivity of the soil in lateral direction and bedrock conductivity, b) conductivity of the soil in vertical direction and bedrock conductivity. Note the logarithmic *x*-axis.

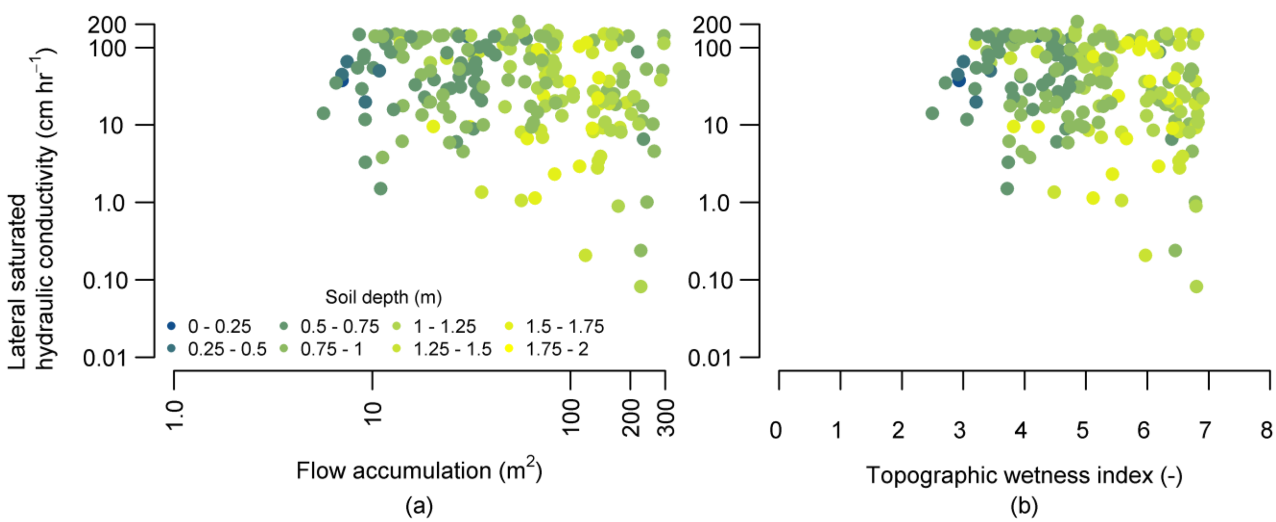

Fig. 4. Lateral soil saturated hydraulic conductivity plotted versus (a) the flow accumulation area of the bedrock topography and (b) topographic wetness index (TWI) of the bedrock topography. For both flow accumulation area and TWI, the 80-percentile value of all points within 1 m radius of each well was used. The color coding indicates average soil depths around the wells.

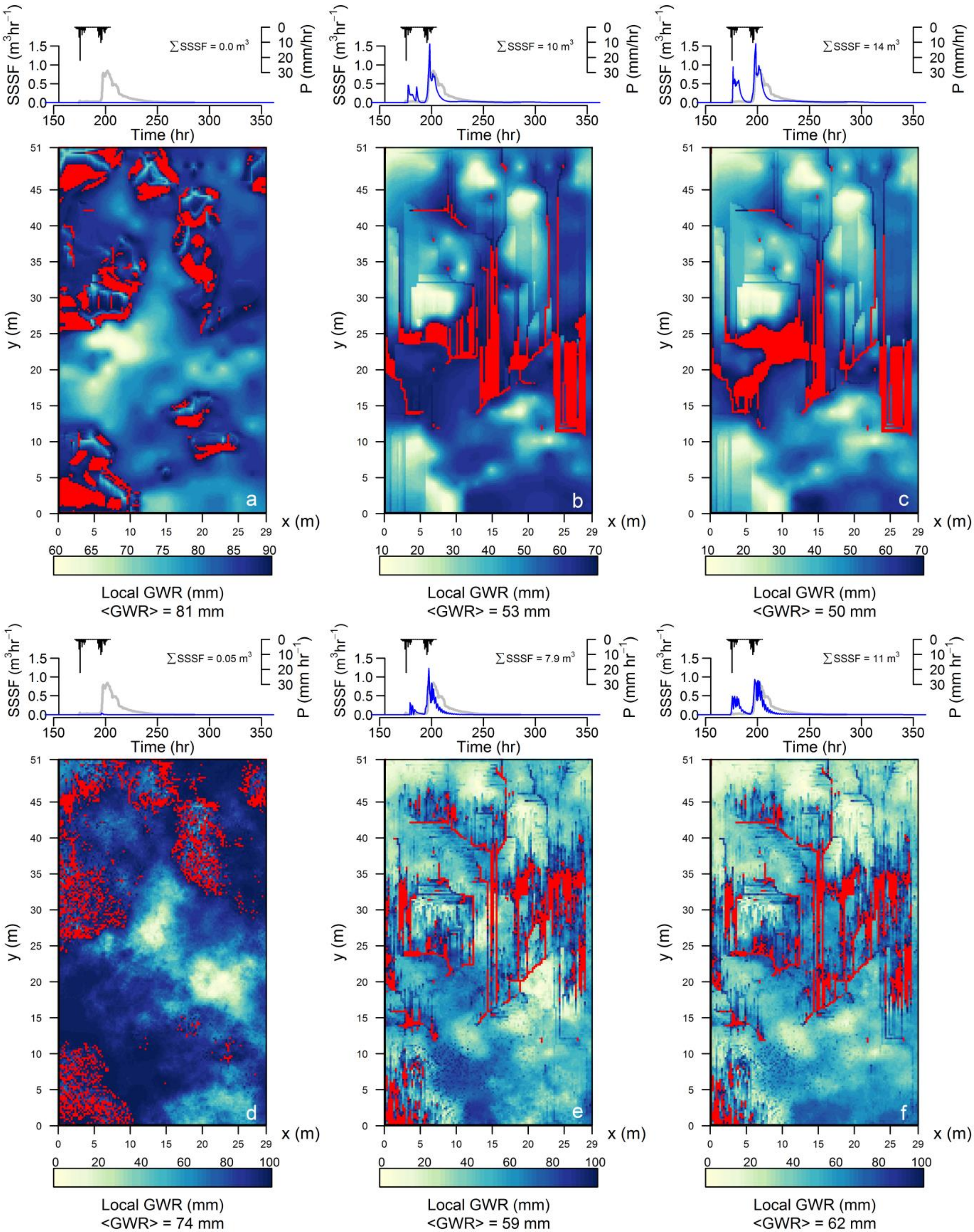

Fig. 5. Hydrographs and maps of bedrock groundwater recharge after the 6-7 March 1996 rain storm. The grey line is the observed hydrograph in the trench, the black line the input precipitation and the blue line the hydrograph of subsurface flow at the bottom of the model domain. The maps show cumulative bedrock groundwater recharge from the start of the rain storm until the end of the simulation (7 days) in every grid cell. The color scales vary between the simulations. The red dots

indicate locations with bedrock groundwater recharge higher than the 90-percentile value. The simulations of panels a-c were performed with spatially uniform K_V, K_L, and K_{BR} (values presented in Table 2), those of panels d-f with spatially variable fields of K_V, K_L, and K_{BR} (values presented in Table 2).

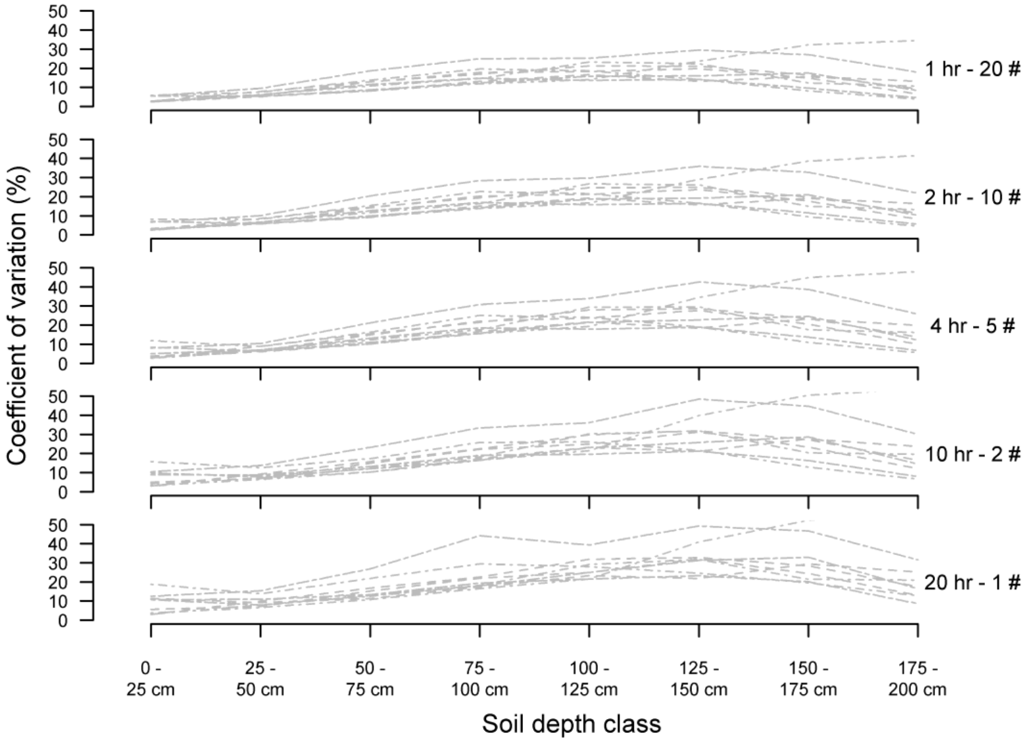

Fig. 6. Coefficient of variation of groundwater recharge (%) determined in 8 classes of soil depth. Each panel contains the results of a precipitation scenario presented in Table 1 (forcing of simulation set 2). A precipitation scenario consists of 100 mm rain applied at a rate of 5 mm hr^{-1}, but in a varying number of storms within the simulation (with storm duration increasing while the number of storms in the simulation decreases). Each grey line represents one of 25 simulations with a random combination of K_V, K_L, and K_{BR}. For clarity only twelve out of 25 simulations have been plotted.

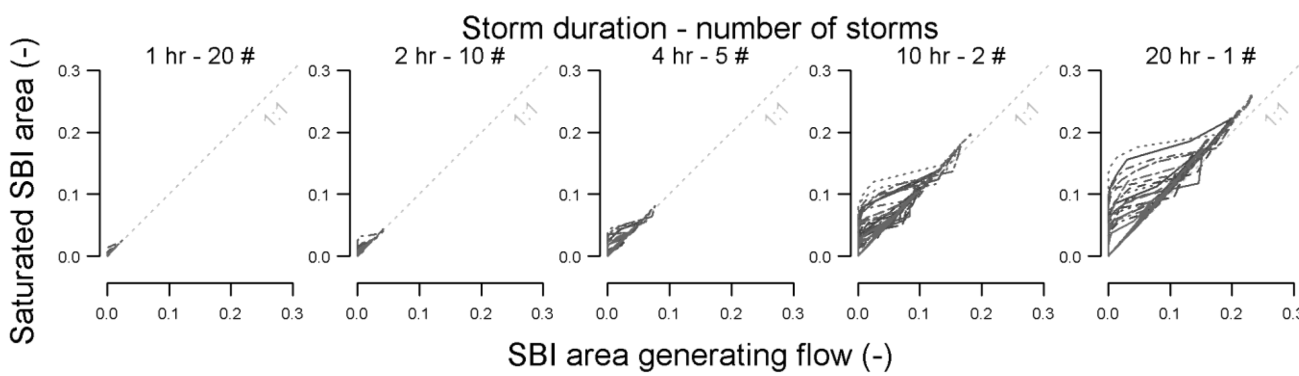

Fig. 7. Saturated areal fraction of SBI plotted against the areal fraction of SBI where the percolation rate is larger than K_{BR} and subsurface lateral flow is generated. Each line represents one of 25 simulations with a random combination of K_V, K_L, and K_{BR}.

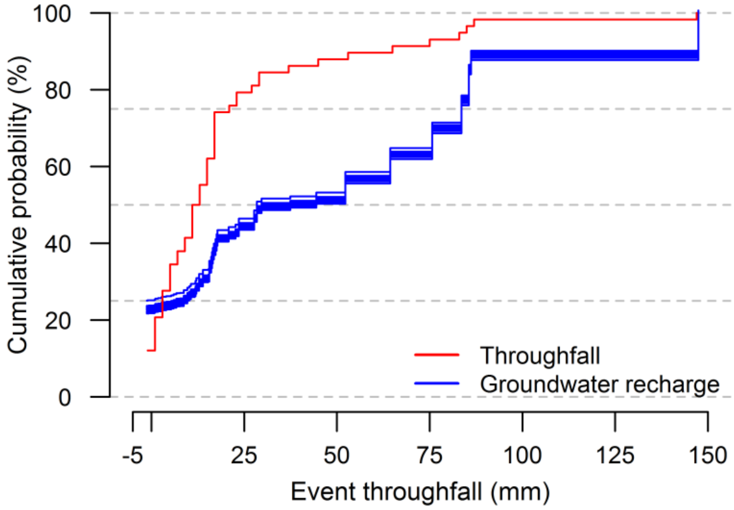

Fig. 8. Cumulative distribution of annual bedrock groundwater recharge and throughfall as a function of event throughfall amount for all 25 simulations. A negative event throughfall indicates net transpiration in the current event definition.

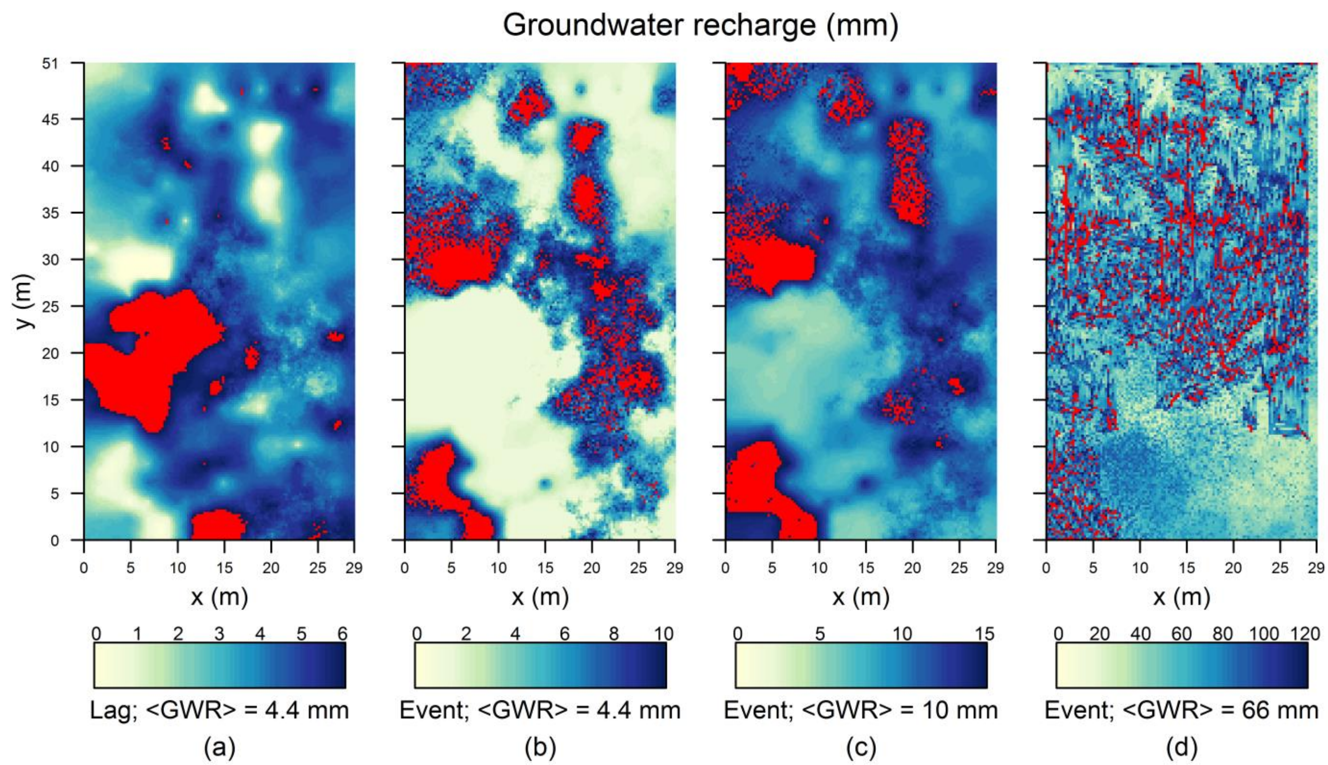

Fig. 9. Maps of cumulative groundwater recharge of one lag between rain events and three events of increasing size (a-d). Every color scale is cut off at the 90-percentile value of groundwater recharge during the specific period. The locations in red are the locations where GWR is larger than the 90-percentile value. An event was defined as rainstorm duration plus the following 24 dry hours. A lag was defined as a dry period beyond those 24 hours until the start of the subsequent rainstorm.

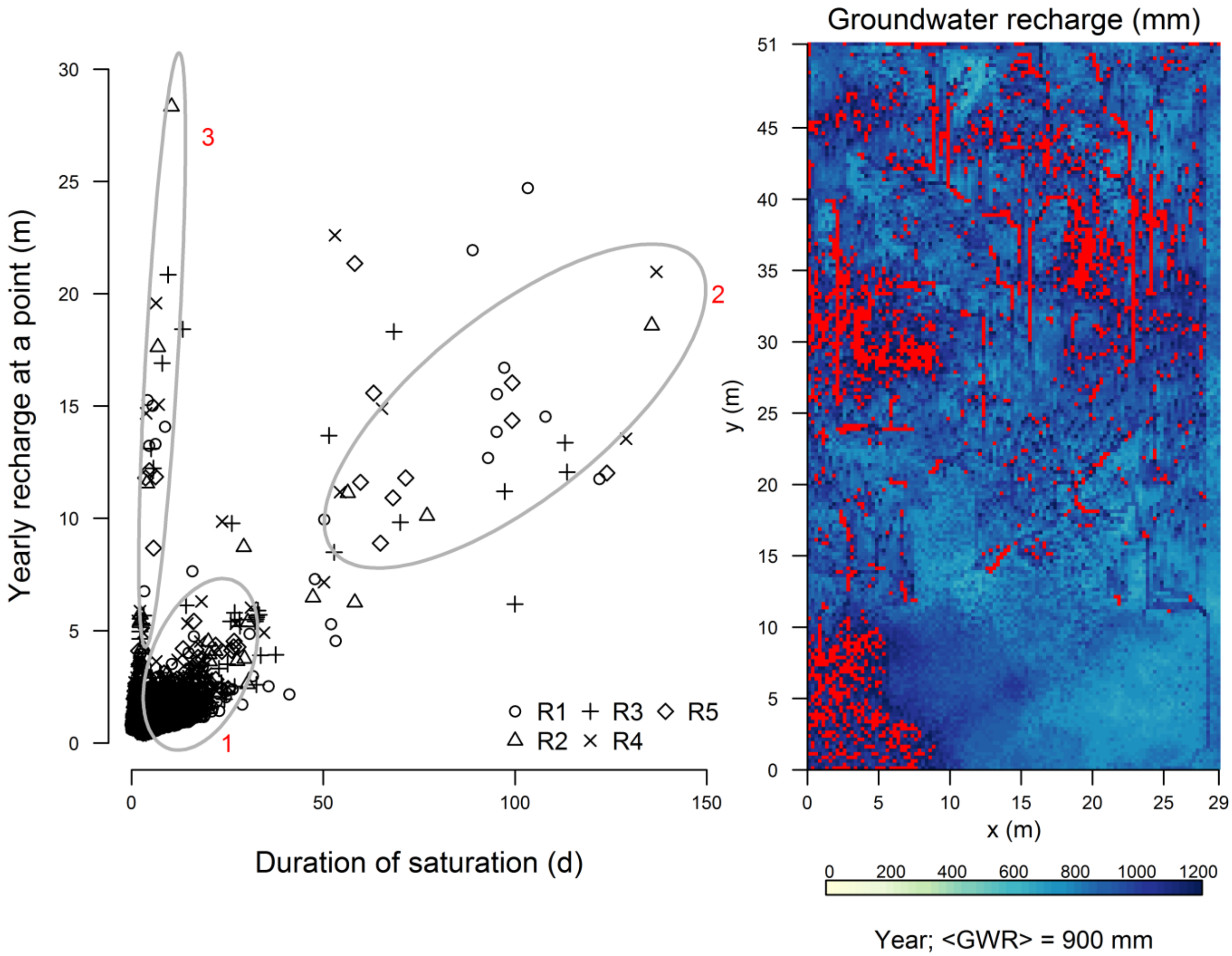

Fig. 10. Cumulative groundwater recharge at a point as a function of the duration of saturation for five random realizations (left, realizations indicated with different symbols. Map of yearly cumulative groundwater recharge (right). The color scale was cut off at the 90-percentile value of groundwater recharge and the locations with higher GWR colored red.

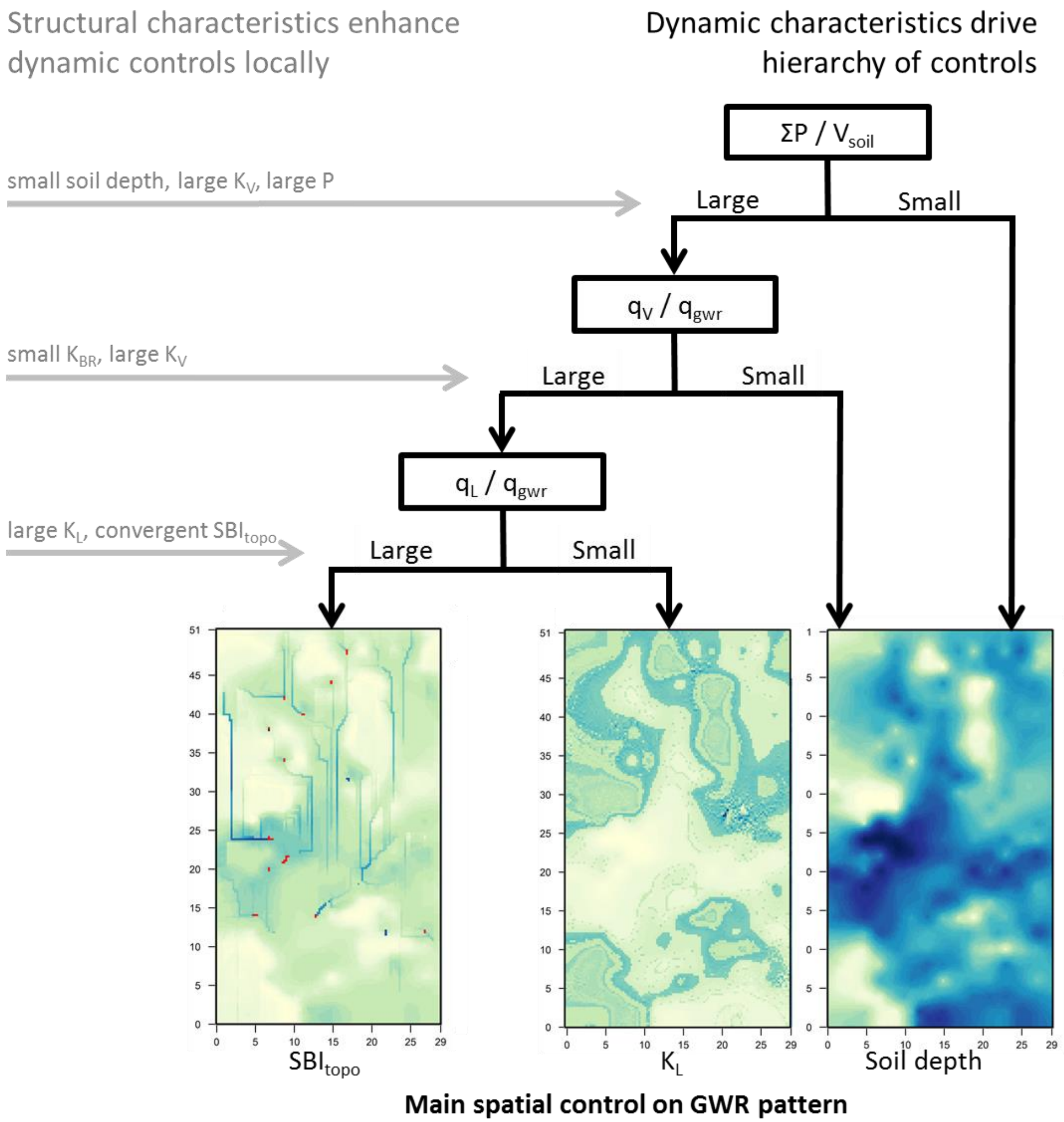

817
818 Fig. 11. Conceptual model of generation of a spatial pattern of groundwater recharge at the Panola hillslope. The structural
819 characteristics that reinforce the effect of a dynamic control are indicated in grey on the left side of the figure.